# Residence Time Distribution in a Single-Phase Rotor–Stator Spinning Disc Reactor

**Frans Visscher, Jos de Hullu, Mart H. J. M. de Croon, John van der Schaaf, and Jaap C. Schouten**
Laboratory of Chemical Reactor Engineering, Dept. of Chemical Engineering and Chemistry,
Eindhoven University of Technology, 5600 MB Eindhoven, The Netherlands

*DOI 10.1002/aic.14036*
*Published online February 25, 2013 in Wiley Online Library (wileyonlinelibrary.com)*

*A reactor model for the single-phase rotor–stator spinning disc reactor based on residence time distribution measurements is described. For the experimental validation of the model, the axial clearance between the rotor and both stators is varied from $1.0 \times 10^{-3}$ to $3.0 \times 10^{-3}$ m, the rotational disc speed is varied from 50 to 2000 RPM, and the volumetric flow rate is varied from $7.5 \times 10^{-6}$ to $22.5 \times 10^{-6}$ $m^3$ $s^{-1}$. Tracer injection experiments show that the residence time distribution can be described by a plug flow model in combination with 2–3 ideally stirred tanks-in-series. The resulting reactor model is explained with the effect of turbulence, the formation of Von Kármán and Bödewadt boundary layers, and the effect of the volumetric flow rate.* © 2013 American Institute of Chemical Engineers *AIChE J*, 59: 2686–2693, 2013
*Keywords: residence time distribution, fluid flow modeling, rotor–stator spinning disc reactor*

## Introduction

Numerical characterization of the macromixing behavior in chemical reactors can be made when the residence time distribution (RTD) in the reactors is known.[1] The RTD can be determined from tracer injection experiments[2–7] and has been characterized for different reactors like microchannel reactors,[8] foam packed trickle flow reactors,[9] annular centrifugal extractors,[10] and the rotating disc reactor.[11] In this article, we present a single-phase model for a rotor–stator spinning disc reactor (SDR), which is based on residence time distribution measurements.

The SDR consists of a rotating disc (rotor) with two stationary discs (stators). The rotor and stators are located at low axial clearance, typically in the range of millimeters. The configuration is schematically shown in Figure 1. Due to the difference in rotational disc speed, a velocity gradient is present between the rotor and the stators, causing a high shear force to act on the fluid between the rotor and stators. For liquid–liquid, liquid–solid, and gas–liquid mixtures, this results in a large interfacial area and an increase of the turbulence intensity, which yields mass-transfer rates up to 20 times higher than those measured for conventional multiphase reactors.[12–17] The gas–liquid mass-transfer rate was described by a model that is based on a combination of ideally stirred tanks and plug flow.[18] Multiple discs were mounted on a single rotational axis to obtain ideally stirred tanks-in-series, which ultimately will lead to more plug flow behavior of the fluid flow in the reactor.[7,19] Therefore, this reactor is a promising tool to achieve process intensification goals, for example, realize a reduction of equipment volume, enhance volumetric productivity, and increase of mass-transfer rates in continuous flow reactors.

This article presents the residence time distribution in the rotor–stator spinning disc reactor as a function of the rotational disc speed, axial disc spacing, and the volumetric flow rate. Based on the RTD measurements, a single-phase model is described as the combination of a plug flow model and a number of tanks-in-series. With the RTD known, the feasibility of industrial implementation can be evaluated.[20]

## Experimental Procedure

### Materials

Demineralized water was used for all experiments. The water was demineralized with a Millipore Elix UV-10. Pelikan® Royal Blue fountain pen ink was used as a tracer for the water phase and supplied by BETO Schoolartikelen. All experiments were performed at ambient lab temperature, $292 \pm 2$ K.

### Experimental set-up

The rotor–stator spinning disc reactor was previously described by Meeuwse et al. (Figure 1).[15] The stationary reactor wall has an inner radius of 0.145 m. The top stator and the rotor are made of stainless steel. The bottom stator is made of polymethyl methacrylate for visualization purposes. The rotor is made of stainless steel and has an outer radius of 0.135 m and a thickness of $4 \times 10^{-3}$ m. The spacing between the rotor and the stators, further denoted as disc spacing, is equal for the top and bottom stator and can be adjusted by changing the height of the stators. The applied disc spacings are $h = 1.0 \times 10^{-3}$ m, $h = 2.0 \times 10^{-3}$ m, and $h = 3.0 \times 10^{-3}$ m. The rotational disc speed ranged from 50 to 2000 RPM. The water flow rate, $Q$, ranged from

Additional Supporting Information may be found in the online version of this article.

Contract grant sponsor: European Research Council; Contract grand number: 227010.

Correspondence concerning this article should be addressed to J. C. Schouten at J.C.Schouten@tue.nl.

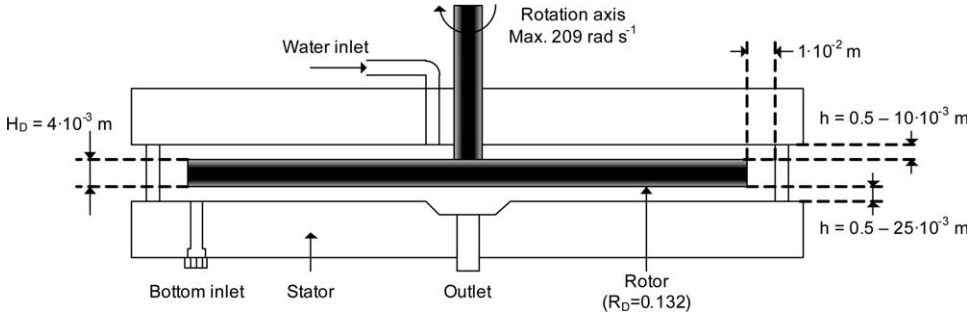


**Figure 1. Schematic side view of the rotor–stator spinning disc reactor.**

**The reactor volume equals 167 × $10^{-6}$ $m^3$ at $h = 1.0 \times 10^{-3}$ m, 299 × $10^{-6}$ $m^3$ at $h = 2.0 \times 10^{-3}$ m and 431 × $10^{-6}$ $m^3$ at $h = 3.0 \times 10^{-3}$ m.**

7.5 × $10^{-6}$ $m^3$ $s^{-1}$ to 22.5 × $10^{-6}$ $m^3$ $s^{-1}$ and was controlled by a CORI-FLOW® M55 mass flow controller from Bronkhorst®. All operational data were acquired through LabView 9. The heat dissipated due to the shear forces in the reactor was removed by precooling the water, using a Lauda WKL-1200 cooling system with ethylene glycol as coolant. The complete set-up is schematically shown in Figure 2.

### *Tracer*

Ink was injected by a 25 × $10^{-6}$ $m^3$ Cetoni® Nemesys Syringe pump, through a 1/4″ Swagelok® T-piece at 7 × $10^{-2}$ m from the reactor inlet. At 3.0 × $10^{-2}$ m after the injection point a 1/4″ stainless steel in-line UV–VIS flow cell from Avantes® was connected, with an optical path length of 5 × $10^{-3}$ m. At 3 × $10^{-2}$ m below the reactor outlet, a 1/2″ in-line flow cell from Avantes® was connected with an optical path length of 10 × $10^{-3}$ m. A dual channel AvaSpec-2048-USB2 UV-VIS spectrophotometer was used, which was equipped with an AvaLight-DH-S light source. Lamp, spectrophotometer, and flow cells were connected through 600 × $10^{-6}$ m diameter fibers, with a solar resistant coating. The total volume of the inlet and outlet tubing is equal to 4.3 × $10^{-6}$ $m^3$ $s^{-1}$. The absorbance of the Pelikan Royal Blue ink was measured at 306 nm. A calibration curve was made to ensure that linear range of Lambert–Beer's law was obeyed (Supporting Information). The applied pulse (injected volume 50 × $10^{-9}$, 100 × $10^{-9}$, and 200 × $10^{-9}$ $m^3$ and injection rate 50 × $10^{-9}$, 100 × $10^{-9}$, and 200 × $10^{-9}$ $m^3$ $s^{-1}$) was examined to ensure reproducible injections with an optimal Dirac character, in which peak tailing was minimized (Supporting Information). All tracer injections were performed by injecting 200 × $10^{-9}$ $m^3$ ink at 200 × $10^{-9}$ $m^3$ $s^{-1}$. The tracer injection took place over a period that is short compared with residence times of the reactor, that is, less than 4%. At each experimental condition, two successive injections were performed. Data from successive measurements were collected through LabView® every 0.50 s during the period of successive measurements and analyzed using MatLab®. A standard MatLab® routine (Findpeaks) was used to separate successive measurements, which separates measurements based on a minimal time difference between peaks, minimum height difference in peaks, and a minimum height between peaks.

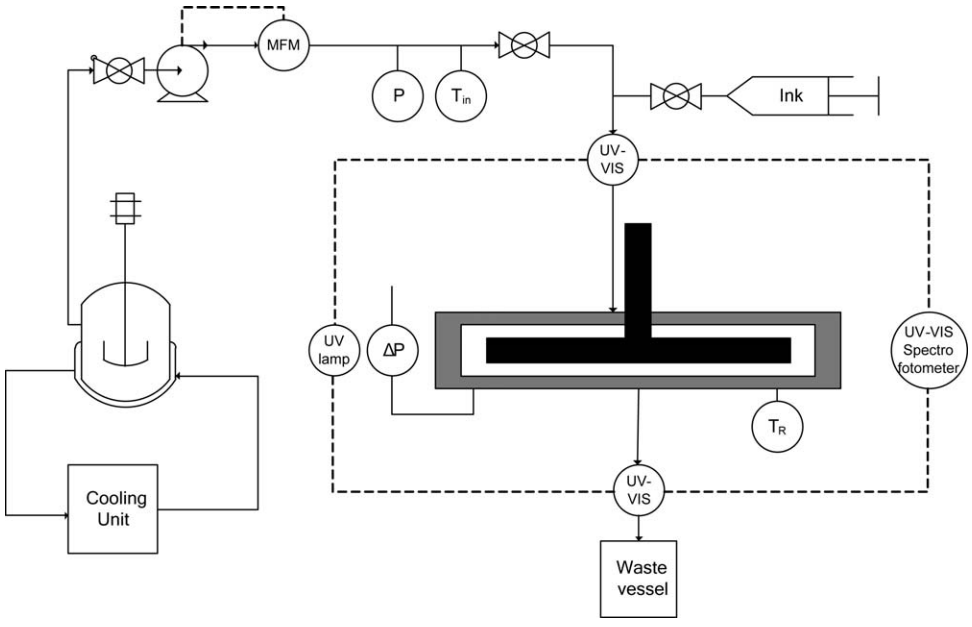


**Figure 2. Experimental set-up with all additional equipment.**

**All tubing is made out of 1/4″ Swagelok® tubing. All operational data are controlled and monitored through a LabView® application. Data work up is done through MatLab®.**

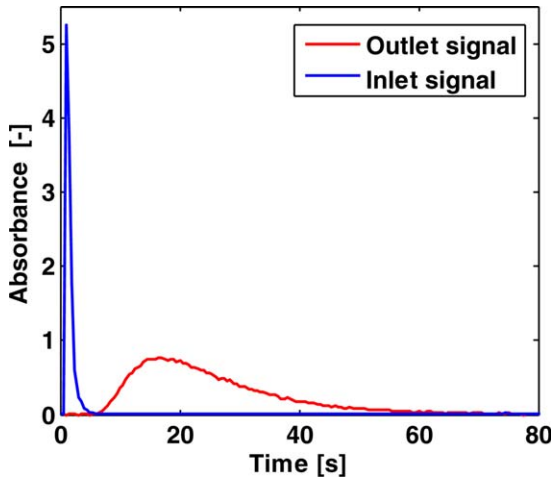


**Figure 3. The measured absorbance at the inlet and outlet signal is shown for a pulse, under the experimental condition $Q = 7.5 \times 10^{-6}$ m$^3$ s$^{-1}$, $\Omega = 250$ RPM, and $h = 1.0 \times 10^{-3}$ m.**

**[Color figure can be viewed in the online issue, which is available at wileyonlinelibrary.com.]**

Equation 1 shows how the residence time distribution function, $E(t)$, is calculated from the tracer concentration at the reactor outlet.

$$E(t) = \frac{C(t)}{\int_0^\infty C(t)dt} \tag{1}$$

The integral in the denominator of Eq. 1 is calculated through trapezoidal numerical integration. The limits of the integration interval are deduced from the maximum absorbance and the average base line absorbance of the outlet signal. The integration interval is calculated for each separate measurement. The lower integration limit of the integral in Eq. 1 is given by the last time step before the maximum absorbance in the outlet signal, at which the absorbance is equal to the average baseline absorbance. The upper integration limit is given by the first time step after the maximum absorbance in the outlet signal is detected, at which the absorbance is at the baseline absorbance. When the integration interval exceeds six times the residence time ($\tau = V_R/Q$), the measurement is discarded to prevent tailing dominated measurements.[21–24] Less than 2% of the measurements were discarded.

## Results and Discussion

### *Tracer detection*

The ink pulse at the inlet was measured $3 \times 10^{-2}$ m before the reactor in the $^1/_4''$ in-line flowcell and $3 \times 10^{-2}$ m after the reactor outlet in the $^1/_2''$ in-line flowcell. Between two injections, at least 10 s of steady-state signal at the absorbance baseline level was awaited, to ensure a good distinction between the consecutive measurements. The measured absorbance at the inlet and outlet is given in Figure 3. The injection of the tracer causes a sharp increase of the tracer concentration at the reactor inlet. Only one peak is observed after tracer injection, thus, channeling is absent. From Figure 3, it is concluded that the reactor can be

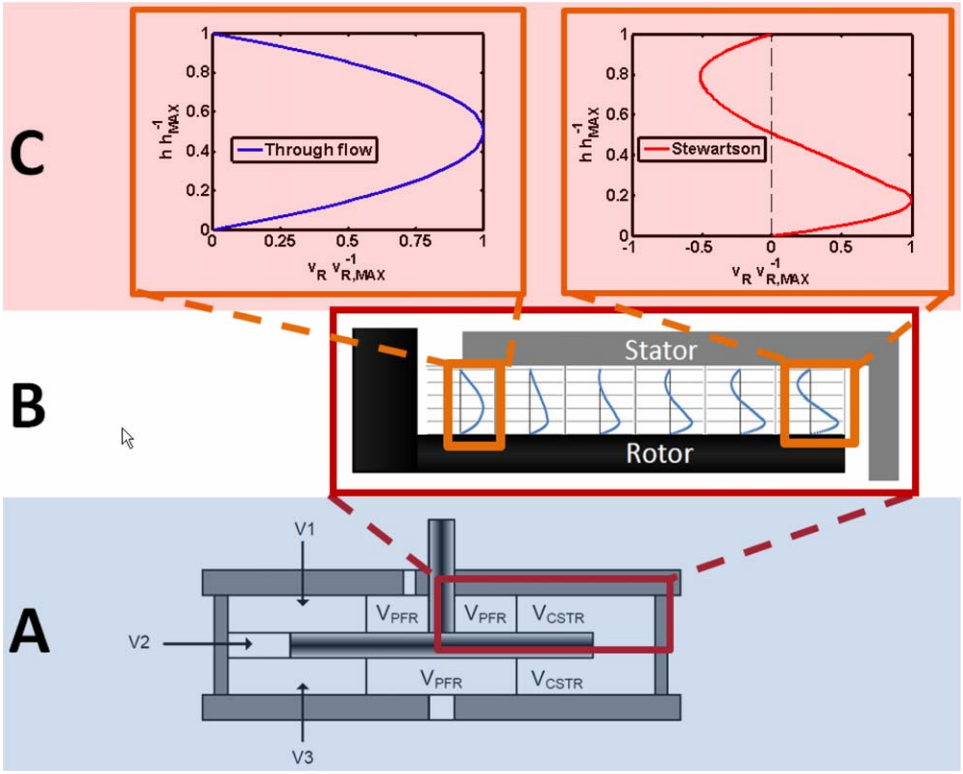


**Figure 4. (A) Reactor model that described the single-phase fluid flow in the spinning disc reactor; (B) the transition of the though flow governed radial velocity profile to the boundary layer governed radial velocity profile; (C) the through flow and boundary layer governed radial liquid velocity profiles.**

**[Color figure can be viewed in the online issue, which is available at wileyonlinelibrary.com.]**

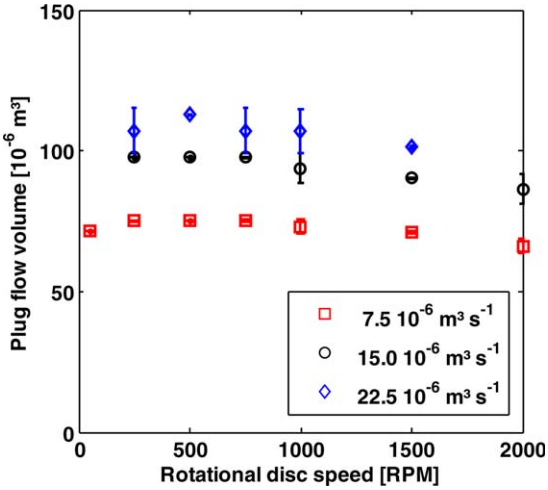


**Figure 5. Rotational disc speed vs. the plug flow volume at a disc spacing of 1.0 × $10^{-3}$ m, for different volumetric flow rates.**

**[Color figure can be viewed in the online issue, which is available at wileyonlinelibrary.com.]**

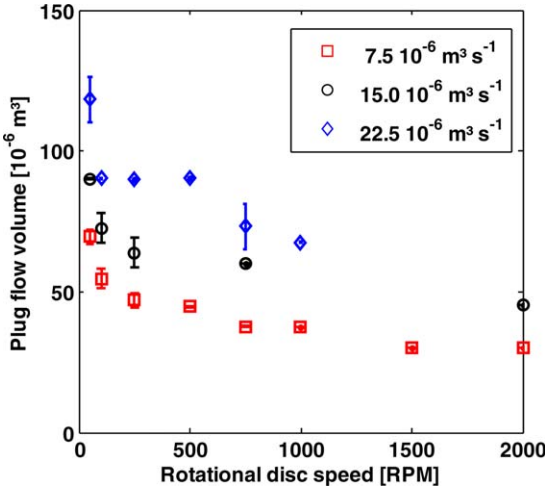


**Figure 7. Rotational disc speed vs. the plug flow volume at a disc spacing of 3.0 × $10^{-3}$ m, for different volumetric flow rates.**

**[Color figure can be viewed in the online issue, which is available at wileyonlinelibrary.com.]**

modeled as a plug flow volume in combination with a mixed volume. The plug flow volume is further denoted as $V_{PFR}$, the mixed volume as $V_{CSTR}$. The corresponding residence times equal $\tau_{PFR}$ $(=V_{PFR}Q^{-1})$ and $\tau_{CSTR}$ $(=V_{CSTR}Q^{-1})$, respectively. The residence time of the plug flow volume, $\tau_{PFR}$, is calculated from the difference between the points in time at which the tracer is first detected at the reactor inlet and outlet, respectively.

### *Plug flow volume*

The SDR can be modeled as a combination of a plug flow volume with a mixed volume, as is shown in Figure 4A. $V_{PFR}$ originates from the volume of the reactor where the radial liquid velocity profile between the rotor and the stator is dominated by the through flow of the liquid phase. The transition is shown in Figure 4B. When the through flow is dominating the velocity profile, the radial liquid velocity profile has a parabolic shape over the height between the rotor and the stator. This is shown in Figure 4C. $V_{PFR}$ is shown as a function of the rotational disc speed, for the measurements at $h = 1.0 \times 10^{-3}$ m in Figure 5. For all investigated flow rates, that is, $7.5 \times 10^{-6}$ m$^3$ s$^{-1}$, $15.0 \times 10^{-6}$ m$^3$ s$^{-1}$, and $22.5 \times 10^{-6}$ m$^3$ s$^{-1}$, it is decreasing with the rotational disc speed. The decrease is small, that is, 6% for $Q = 22.5 \times 10^{-6}$ m$^3$ s$^{-1}$, 7% for $Q = 15.0 \times 10^{-6}$ m$^3$ s$^{-1}$, and 5% for $Q = 7.5 \times 10^{-6}$ m$^3$ s$^{-1}$. $V_{PFR}$ increases with an increase of the flow rate. At 250 RPM, $V_{PFR}$ increases from $75 \times 10^{-6}$ m$^3$ at $7.5 \times 10^{-6}$ m$^3$ s$^{-1}$ to $11 \times 10^{-5}$ m$^3$ at $22.5 \times 10^{-6}$ m$^3$ s$^{-1}$. As a percentage of the total reactor volume this equals an increase of 45% at $7.5 \times 10^{-6}$ m$^3$ s$^{-1}$ to 64% at $22.5 \times 10^{-6}$ m$^3$ s$^{-1}$. $V_{PFR}$ is shown as a function of the rotational disc speed, for the measurements at $h = 2.0 \times 10^{-3}$ m in Figure 6. As observed for $h = 1.0 \times 10^{-3}$ m, it decreases as a function of the rotational disc speed, whereas it increases with increasing flow rate. The $V_{PFR}$ decrease as a function of the rotational disc speed is larger for the

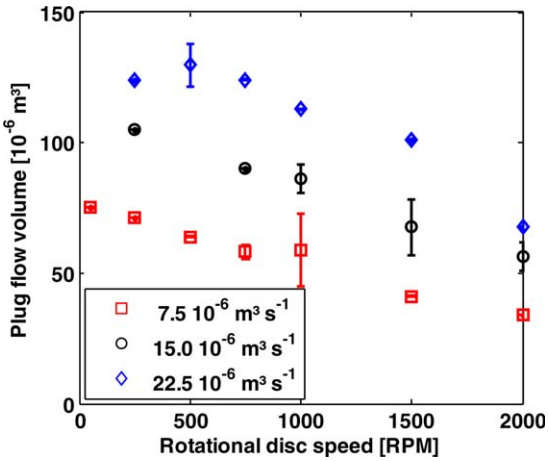


**Figure 6. Rotational disc speed vs. the plug flow volume at a disc spacing of 2.0 × $10^{-3}$ m, for different volumetric flow rates.**

**[Color figure can be viewed in the online issue, which is available at wileyonlinelibrary.com.]**

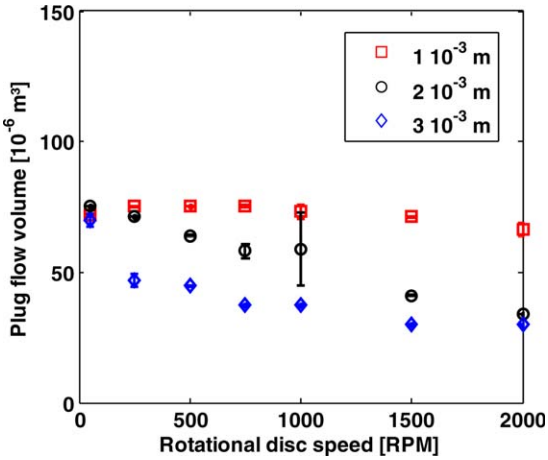


**Figure 8. Rotational disc speed vs. the plug flow volume at a volumetric flow rate of 7.5 × $10^{-6}$ m$^3$ s$^{-1}$, for varying disc spacings.**

**[Color figure can be viewed in the online issue, which is available at wileyonlinelibrary.com.]**

measurements at $h = 2 \times 10^{-3}$ m than those for $h = 1 \times 10^{-3}$ m. The decrease of $V_{PFR}$ equals 46% for $Q = 22.5 \times 10^{-6}$ m$^3$ s$^{-1}$, 47% for $Q = 15.0 \times 10^{-6}$ m$^3$ s$^{-1}$, and 53% for $Q = 7.5 \times 10^{-6}$ m$^3$ s$^{-1}$. $V_{PFR}$ increases with an increase of the flow rate. At 250 RPM, $V_{PFR}$ increases from 71 $\times 10^{-6}$ m$^3$ at $7.5 \times 10^{-6}$ m$^3$ s$^{-1}$ to $120 \times 10^{-6}$ m$^3$ at $22.5 \times 10^{-6}$ m$^3$ s$^{-1}$. As a percentage of the total reactor volume this equals an increase of 24% at $7.5 \times 10^{-6}$ m$^3$ s$^{-1}$ to 41% at $22.5 \times 10^{-6}$ m$^3$ s$^{-1}$. Figure 7 shows $V_{PFR}$ as a function of the rotational disc speed, for measurements at $h = 3.0 \times 10^{-3}$ m. As observed for $h = 1.0 \times 10^{-3}$ m and $2.0 \times 10^{-3}$ m, $V_{PFR}$ decreases as a function of the rotational disc speed and increases with increasing flow rate. The decrease as a function of the rotational disc speed is larger than for $h = 1.0 \times 10^{-3}$ m and $h = 2.0 \times 10^{-3}$ m. For the disc spacings $h = 1.0 \times 10^{-3}$ m, $h = 2.0 \times 10^{-3}$ m, and $h = 3.0 \times 10^{-3}$ m, $V_{PFR}$ is shown as a function of the rotational disc speed in Figure 8 for measurements performed at $Q = 7.5 \times 10^{-6}$ m$^3$ s$^{-1}$. The decrease in $V_{PFR}$ is the strongest for the largest disc spacing.

### *Transition of plug flow to mixed volume*

The SDR can be modeled as a combination of a plug flow volume, $V_{PFR}$, with a mixed volume, $V_{CSTR}$. $V_{PFR}$ originates from the through flow governed radial liquid velocity profile. In the mixed volume, the radial velocity profile of the liquid is dominated by boundary layer formation. In a rotor–stator configuration, two boundary layers exist. The centrifugal von Kármán boundary layer is present at the rotor.[25] The centripetal Bödewadt boundary layer is present at the stator.[26] The boundary layers are merged for small axial disc spacings.[27] For larger axial disc spacings, these boundary layers are separated by a core with a constant angular velocity, as was suggested by Batchelor.[28] Daily and Nece identified four single-phase flow profiles, depending on the rotational disc speed and the disc spacing.[29–31] The flow is laminar (Regimes I and II) or turbulent (Regimes III and IV) with either merged boundary layers (Regimes I and III), or with a central core between the boundary layers (Regimes II and IV). The SDR is always operated in the turbulent regime where boundary layers are merged, that is, regime III.[31] The transition of laminar flow to turbulent flow in absence of through flow, for the merged boundary layers regime was studied by Cros et al.[32–34] The regime with turbulent flow with merged boundary layers was extensively investigated by Haddadi and Poncet.[35] Boundary layer formation in rotor–stator configurations is determined by the rotational disc speed, $\Omega$,[36] disc radius, $R$, kinematic viscosity, $\upsilon$, the axial clearance between the rotor, and the stators, $h$,[37] and the superimposed through flow, $Q$.[38] Also the prerotation of the liquid,[39] and the presence and spacing of a cylindrical enclosure are important.[40]

Owen and Rogers report that with radial centripetal or centrifugal through flow, near the axis boundary layers break down, and that a through flow governing flow profile remains.[41] This is consistent with the experimental findings of Haddadi and Poncet.[35] When the centrifugal von Kármán and centripetal Bodewadt boundary layers are fully developed, the parabolic shape of the radial velocity profile is broken down. Both the experimental and modeling results of Haddadi et al. illustrate that the volumetric through flow in the stator boundary layer increases, when the rotational Reynolds number is increased from $1.8 \times 10^5$ to $5.0 \times 10^6$.[35]

The increase of the radially inward oriented flow in the boundary layer on the stator causes an increase of back mixing and, thus, a decrease of $V_{PFR}$. The disc radius where the boundary layer breaks down the parabolic flow profile depends on the through flow, disc spacing, and the rotational disc speed. With an increase of the rotational disc speed, the boundary layer formation is developed closer to the rotational axis. This explains the decrease of $V_{PFR}$ as a function of the rotational disc speed. When, as an approximation, a constant radial velocity profile of the liquid is assumed over the reactor height, the radial liquid velocity is given by Eq. 2

$$v_r = \frac{Q}{2\pi R h} \tag{2}$$

According to Eq. 2, for a through flow of $7.5 \times 10^{-6}$ m$^3$ s$^{-1}$, the liquid velocity at the entrance, that is, $R = 2.6 \times 10^{-2}$ m, is more than five times higher than at the rim of the disc, that is, $R = 0.135$ m. At a fixed rotational disc speed and disc spacing, for higher volumetric through flow, the liquid velocity is increased. This leads to an increase of the volume where the boundary layer is suppressed, and the through flow is dominating the velocity profile. Thus, $V_{PFR}$ increases. This is in accordance with the trends observed in Figures 5–7. Equation 2 also shows that the radial velocity of the liquid decreases when the disc spacing is increased. This decrease in radial liquid velocity implies that the through flow governed profile is broken down at a radius closer to the rotational axis. This means that $V_{PFR}$ decreases. This is in accordance with the results shown in Figure 8.

### *Mixed volume*

The normalized RTD-function is used to describe and compare the mixed volume of different reactors: $E(\theta) = t_m E(t)$, where $t_m$ is the mean residence time and $\theta$ the dimensionless time, $t\ t_m^{-1}$. The mean residence time and the variance, $\sigma$, around this mean are given by Eqs. 3 and 4. The limit of the integration interval is equal to that used for Eq. 1.

$$t_m = \int_0^\infty t E(t) dt \tag{3}$$

$$\sigma^2 = \int_0^\infty (t - t_m)^2 E(t) dt \tag{4}$$

The $E(\theta)$-curve for $N$ tanks-in-series, with equal volumes $V_{TANK}$, is given by Eq. 5.[2]

$$E(\theta) = \frac{N^N \theta^{N-1}}{(N-1)!} e^{-N\theta} = \frac{N^N \theta^{N-1}}{\int_0^\infty z^{N-1} e^{-z} dz} e^{-N\theta} \tag{5}$$

The $E(\theta)$-curve of the mixed volume is shown in Figure 9, together with a fit of two tanks-in-series with equal volumes. The sum of $\tau_{PFR}$ and $t_m$ was compared with the residence time ($\tau = V_R/Q$). Over all measurements, the resulting volume accounted for at least 94% of the total reactor volume. This difference could be caused by a dead volume.[42] This dead volume would originate from a stagnant zone, which could be located where the horizontal bottom stator is attached to the vertical cylindrical housing.

The error bars in the Figures 5–8 represent the standard deviation in $V_{PFR}$. This standard deviation is calculated from the duplicate experiments and was less than 10% for most

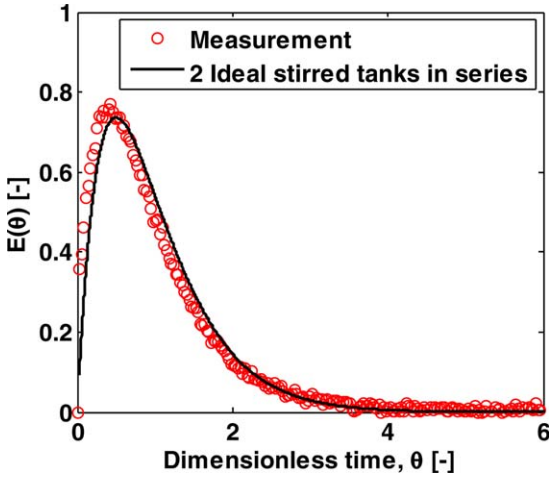


**Figure 9. The $E(\theta)$-diagram of the mixed volume of the outlet signal in Figure 3 is given, together with the fit of the two tanks-in-series model ($t_m = 17.08$ s, $\tau_{PFR} = 5.21$ s, $\tau = 22.3$ s).**

**[Color figure can be viewed in the online issue, which is available at wileyonlinelibrary.com.]**

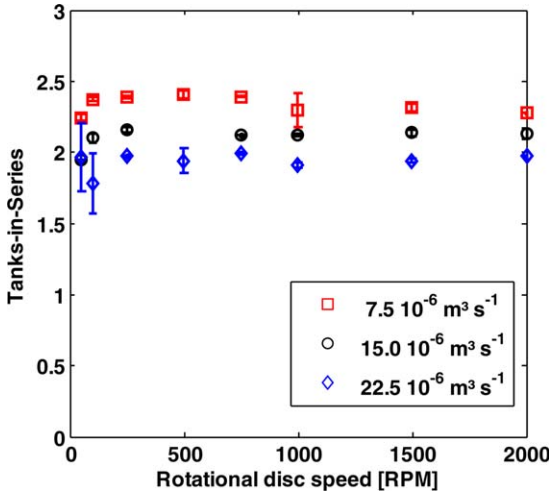


**Figure 11. Rotational disc speed vs. the number of tanks-in-series at a disc spacing of 2.0 × $10^{-3}$ m, for different volumetric flow rates.**

**[Color figure can be viewed in the online issue, which is available at wileyonline library.com.]**

measurements, indicating that the experimental approach leads to reproducible results. The number of tanks-in-series, $N$, with equal volumes can be determined from the variance in Eq. 4 and the mean residence time in Eq. 3, by using Eq. 6. Increasing the upper integration limit of Eq. 1 with $0.5\tau$ results in a value of $N$ which is 6% higher. The error due to the integration limit of Eq. 1 is, thus, smaller than the reproducibility of the duplicate measurements and is, thus, negligible.

$$N = \frac{t_m^2}{\sigma^2} \tag{6}$$

### *Number of tanks-in-series*

The number of tanks-in-series needed to describe the mixed volume for $h = 1.0 \times 10^{-3}$ m is shown in Figure 10, for $h = 2.0 \times 10^{-3}$ m in Figure 11 and for $h = 3.0 \times 10^{-3}$ m in Figure 12. For all disc spacings, the number of tanks-in-series is not dependent on the rotational disc speed. To model the mixed volume of the reactor, 2–2.5 tanks-in-series are needed. This can be understood when the mixed volume in the reactor is described as three tanks-in-series. This model is schematically shown in Figure 4A. One tank is located between the rotor and the top stator (V1). The next tank is formed by the volume aside of the rotor (V2). The last tank is located between the rotor and the bottom stator (V3). For all measurements, the number of tanks-in-series is the largest at the lowest flow rate. For an increasing volumetric flow rate, the interaction of the volumes V1 and V3 with the tank next to the rotor, V2 is increased. Accordingly, the influence of V2 decreases, causing the decrease in the number of tanks-in-series with increasing flow rate. The radial position where boundary layer development starts to

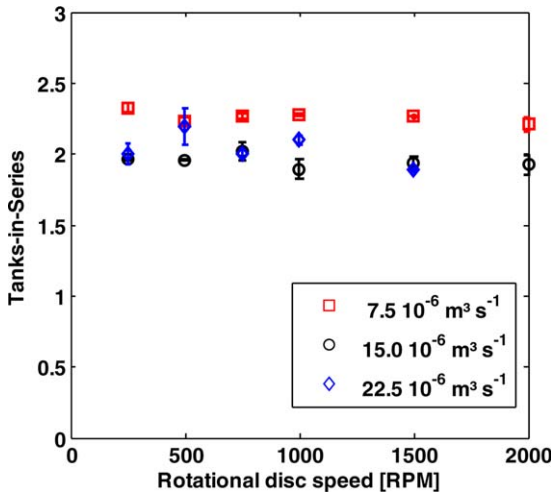


**Figure 10. Rotational disc speed vs. the number of tanks-in-series at a disc spacing of 1.0 × $10^{-3}$ m, for different volumetric flow rates.**

**[Color figure can be viewed in the online issue, which is available at wileyonline library.com.]**

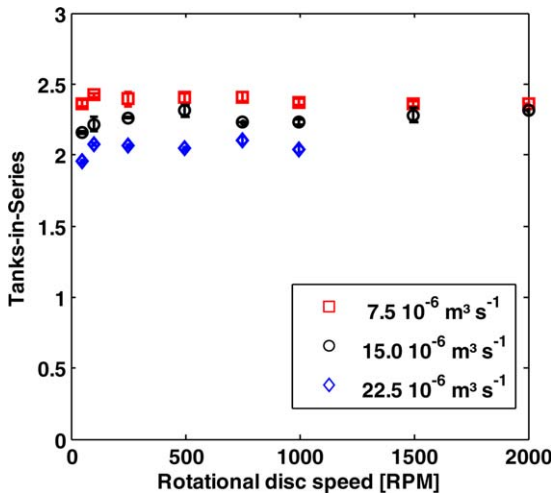


**Figure 12. Rotational disc speed vs. the number of tanks-in-series at a disc spacing of 3.0 × $10^{-3}$ m, for different volumetric flow rates.**

**[Color figure can be viewed in the online issue, which is available at wileyonline library.com.]**

dominate the radial liquid velocity profile does not change the number of tanks-in-series. Therefore, the number of tanks-in-series is not a function of the rotational disc speed.

## Conclusions

This article describes a reactor model based on single-phase residence time distribution measurements in a rotor–stator spinning disc reactor. Measurements are based on the pulse wise injection of a tracer. For the validation of the model, the disc spacing between the rotor and the stators was varied from $1.0 \times 10^{-3}$ to $3.0 \times 10^{-3}$ m, the rotational disc speed was varied from 50 to 2000 RPM, and the volumetric flow rate was varied from $7.5 \times 10^{-6}$ to $22.5 \times 10^{-6}$ m$^3$ s$^{-1}$. The resulting reactor model consists of a plug flow model in combination with a number of tanks-in-series. The volume of the reactor that can be described by a plug flow model decreases as a function of rotational disc speed. This volume increases with the volumetric flow rate. The mixed volume is described as 2–3 of tanks-in-series with equal volumes, which is determined through the mean residence time and the variance of the RTD curve. The number of tanks-in-series can be understood by assuming the volume above and below the rotor as an ideally mixed volume, in combination with a third ideally mixed volume at the rim of the reactor. The reactor model is explained with the development of turbulence, the formation of Von Kármán and Bödewadt boundary layers, and the effect of volumetric flow rates.

## Acknowledgments

This research has received funding from the European Research Council under the European Community's Seventh Framework Programme (FP7/2007-2013)/ERC grant agreement no. 227010 and is gratefully acknowledged.

## Notation

### *Symbols*

$C$ = tracer concentration, mol m$^{-3}$
$E$ = residence time function
$h$ = disc spacing, m
$N$ = number of tanks-in-series with equal volume
$n$ = number of measurement point in RTD-curve
$Q$ = volumetric flow rate, m$^3$ s$^{-1}$
$R$ = radius, m
$t$ = time, s
$t_m$ = mean residence time, s
$V$ = volume of fluid, m$^3$
$v$ = radial liquid velocity, m s$^{-1}$
$z$ = arbitrary integration variable

### *Greek letters*

$\theta$ = dimensionless time, $t\ t_m^{-1}$
$\sigma$ = variance
$\tau$ = residence time, s
$\upsilon$ = kinematic viscosity, m$^2$ s$^{-1}$
$\Omega$ = rotational disc speed, RPM

### *Subscripts*

CSTR = continuous stirred-tank reactor
IN = inlet
PFR = plug flow reactor
R = reactor
r = radius

## Literature Cited

1. Nauman EB. Residence time distributions. In: Paul EL, Atiemo-Obeng VA, Kresta SM, editors. Handbook of Industrial Mixing. Hoboken, NJ: Wiley; 2004:1–17.
2. Levenspiel O. Nonideal Flow. Chemical Rection Engineering, 2nd ed. Hoboken, NJ: Wiley; 1999.
3. Thyn J, Zitny R. Radiotracer applications for the analysis of complex flow structure in industrial apparatuses. *Nucl Instrum Methods Phys Res Sect B*. 2004;213:339–347.
4. Rothfeld LB, Ralph JL. Equivalence of pulse and step residence time measurements in a trickle-phase bed. *AlChE J*. 1963;9(6):852–859.
5. Anderson NG. Using continuous processes to increase production. *Org Process Res Dev*. 2012;16(5):852–869.
6. Danckwerts PV, Jenkins JW, Place G. The distribution of residence-times in an industrial fluidised reactor. *Chem Eng Sci*. 1954;3(1):26–35.
7. Danckwerts PV. Continuous flow systems: distribution of residence times. *Chem Eng Sci*. 1953;2(1):1–13.
8. Thulasidas TC, Abraham MA, Cerro RL. Dispersion during bubble-train flow in capillaries. *Chem Eng Sci*. 1999;54(1):61–76.
9. Saber M, Huu TT, Pham-Huu C, Edouard D. Residence time distribution, axial liquid dispersion and dynamic−static liquid mass transfer in trickle flow reactor containing $\beta$-SiC open-cell foams. *Chem Eng J*. 2012;185–186:294–299.
10. Deshmukh SS, Sathe MJ, Joshi JB, Koganti SB. Residence time distribution and flow patterns in the single-phase annular region of annular centrifugal extractor. *Ind Eng Chem Res*. 2008;48(1):37–46.
11. Jin Kim M, Sung Ghim Y, Nam Chang H. Residence time distribution analysis in controllable flow conditions: case of rotating disk reactor. *Chem Eng Sci*. 1984;39(5):813–819.
12. Meeuwse M, Lempers S, van der Schaaf J, Schouten JC. Liquid–solid mass transfer and reaction in a rotor–stator spinning disc reactor. *Ind Eng Chem Res*. 2010;49(21):10751–10757.
13. Visscher F, van der Schaaf J, de Croon MHJM, Schouten JC. Liquid–liquid mass transfer in a rotor−stator spinning disc reactor. *Chem Eng J*. 2012;185–186:267–273.
14. van der Schaaf J, Schouten JC. High-gravity and high-shear gas-liquid contactors for the chemical process industry. *Curr Opin Chem Eng*. 2011;1(1):84–88.
15. Meeuwse M, Hamming E, van der Schaaf J, Schouten JC. Effect of rotor–stator distance and rotor radius on the rate of gas–liquid mass transfer in a rotor–stator spinning disc reactor. *Chem Eng Process: Process Intens*. 2011;50(10):1095–1107.
16. Meeuwse M, van der Schaaf J, Kuster BFM, Schouten JC. Gas–liquid mass transfer in a rotor–stator spinning disc reactor. *Chem Eng Sci*. 2010;65(1):466–471.
17. Visscher F, Bieberle A, Schubert M, van der Schaaf J, de Croon MHJM, Hampel U, Schouten JC. Water and *n*-heptane volume fractions in a rotor–stator spinning disc reactor. *Ind Eng Chem Res*. 2012;51(51):16670–16676.
18. Meeuwse M, van der Schaaf J, Schouten JC. Mass transfer in a rotor–stator spinning disk reactor with cofeeding of gas and liquid. *Ind Eng Chem Res*. 2009;49(4):1605–1610.
19. Meeuwse M, van der Schaaf J, Schouten JC. Multistage rotor–stator spinning disc reactor. *AlChE J*. 2012;58(1):247–255.
20. Mohammadi S, Boodhoo K. Online conductivity measurement of residence time distribution of thin film flow in the spinning disc reactor. *Chem Eng J*. 2012;207–208:885–894.
21. Torres AP, Oliveira FAR. Residence time distribution studies in continuous thermal processing of liquid foods: a review. *J Food Eng*. 1998;36(1):1–30.
22. Boskovic D, Loebbecke S. Modelling of the residence time distribution in micromixers. *Chem Eng J*. 2008;135(Suppl. 1):S138–S146.
23. Cengroš J, Badin V, Stefan P. Residence time distribution in a wiped liquid film. *Chem Eng J Biochem Eng J*. 1995;59(3):259–263.
24. Martin AD. Interpretation of residence time distribution data. *Chem Eng Sci*. 2000;55(23):5907–5917.
25. Kármán T. Über laminare und turbulente reibung. *Z Angew Math Mech*. 1921;1(4):233–252.
26. Bödewadt UT. Die drehströmung über festem grunde. *Z Angew Math Mech*. 1940;20(5):241–253.
27. van Eeten KMP, van der Schaaf J, Schouten JC, van Heijst GJF. Boundary layer development in the flow field between a rotating and a stationary disk. *Phys Fluids*. 2012;24(3):033601–033618.
28. Batchelor GK. Note on a class of solutions of the Navier-Stokes equations representing steady rotationally-symmetric flow. *Q J Mech Appl Math*. 1951;4(1):29–41.

29. Stewartson K. On the flow between two rotating coaxial disks. *Math Proc Cambridge Philos Soc*. 1953;49(2):333–341.
30. Daily JW, Nece RE. Chamber dimension effects on induced flow and frictional resistance of enclosed disks. *J Basic Eng Trans ASME*. 1960;82:217–232.
31. Djaoui M, Dyment A, Debuchy R. Heat transfer in a rotor–stator system with a radial inflow. *Eur J Mech—B/Fluids* 2005;20(3):371–398.
32. Cros A, Ali R, Le Gal P, Thomas PJ, Schouveiler L, Carpenter PW, Chauve MP. Effects of wall compliance on the laminar–turbulent transition of torsional Couette flow. *J Fluid Mech*. 2003;481:177–186.
33. Cros A, Le Gal P. Spatiotemporal intermittency in the torsional Couette flow between a rotating and a stationary disk. *Phys Fluids*. 2002;14(11):3755–3765.
34. Schouveiler L, Le Gal P, Chauve MP. Instabilities of the flow between a rotating and a stationary disk. *J Fluid Mech*. 2001;443:329–350.
35. Haddadi S, Poncet S. Turbulence modeling of torsional couette flows. *Int J Rotating Machinery*. 2008;2008:1–27.
36. Itoh M, Yamada Y, Imao S, Gonda M. Experiments on turbulent flow due to an enclosed rotating disk. *Exp Therm Fluid Sci*. 1992;5(3):359–368.
37. Poncet S, Chauve MP, Schiestel R. Batchelor versus Stewartson flow structures in a rotor–stator cavity with throughflow. *Phys Fluids*. 2005;17(7):075110–075115.
38. Poncet S, Chauve MP, Le Gal P. Turbulent rotating disk flow with inward throughflow. *J Fluid Mech*. 2005;522:253–262.
39. Debuchy R, Nour FA, Bois G. An analytical modeling of the central core flow in a rotor–stator system with several preswirl conditions. *J Fluids Eng*. 2010;132(6):061102–061111.
40. Cheah SC, Iacovides H, Jackson DC, Ji H, Launder BE. Experimental investigation of enclosed rotor–stator disk flows. *Exp Therm Fluid Sci*. 1994;9(4):445–455.
41. Owen JM, Rogers RH. Rotor–stator systems with superposed flow. In: Morris WD, editor. Flow and Heat Transfer in Rotating-Disc Systems. Vol. 1. Rotor–stator systems. Somerset, UK: Wiley, 1989.
42. Schuur B, Kraai GN, Winkelman JGM, Heeres HJ. Hydrodynamic features of centrifugal contactor separators: experimental studies on liquid hold-up, residence time distribution, phase behavior and drop size distributions. *Chem Eng Processing: Process Intens*. 2012;55:8–19.

*Manuscript received Sept. 19, 2012, revision received Dec. 10, 2012.*